JBC Papers in Press. Published on January 2, 2014 as Manuscript M113.512285
The latest version is at http://www.jbc.org/cgi/doi/10.1074/jbc.M113.512285

The TRPM6 kinase domain determines the Mg·ATP-sensitivity of TRPM7/M6 heteromeric ion channels*

Zheng Zhang [1,3,&], Haijie Yu [1,&], Junhao Huang[1], Malika Faouzi[1], Carsten Schmitz [2], Reinhold Penner [1@], Andrea Fleig [1@]

[1]From the Laboratory of Cell and Molecular Signaling, Center for Biomedical Research, The Queen's Medical Center and John A. Burns School of Medicine, University of Hawaii, Honolulu, Hawaii 96813

[2] Integrated Department of Immunology, University of Colorado Denver and National Jewish Health, Denver, Colorado, 80206

[3] Present address: Department of Pharmacology, School of Pharmaceutical Sciences, Central South University, Changsha, Hunan 410078, China

*Running Title: Mg·ATP insensitivity of TRPM6/TRPM7 heteromeric ion channels

[&]These authors contributed equally to this work.

[@]To whom correspondence should be addressed: Andrea Fleig or Reinhold Penner, The Queen's Medical Center, 1301 Punchbowl St., Honolulu, HI 96813, U.S.A. e-mail: afleig@hawaii.edu - rpenner@hawaii.edu

Keywords: TRP channels, protein kinase, protein complexes , metabolic regulation, magnesium

Background: TRPM6 and TRPM7 combine ion channel and alpha-kinase functions.

Results: ATP inhibits TRPM7, but not TRPM6 or heteromeric TRPM6/M7 channels. Disruption of phosphorylation activity of TRPM6 kinase re-establishes ATP sensitivity to heteromeric channels.

Conclusion: TRPM6 uncouples heteromeric channels from cellular energy levels.

Significance: The altered characteristics of TRPM6/M7 compared to homomeric TRPM7 may enhance Ca^{2+} and Mg^{2+} transport in tissues co-expressing both proteins.

ABSTRACT

The Transient Receptor Potential Melastatin member 7 (TRPM7) and member 6 (TRPM6) are divalent cation channel kinases essential for magnesium (Mg^{2+}) homeostasis in vertebrates. It remains unclear how TRPM6 affects divalent cation transport and whether this involves functional homomeric TRPM6 plasma membrane channels or heteromeric channel assemblies with TRPM7. We show that homomeric TRPM6 is highly sensitive to intracellular free Mg^{2+} and therefore unlikely to be active at physiological levels of $[Mg^{2+}]_i$. Co-expression of TRPM7 and TRPM6 produces heteromeric TRPM7/M6 channels with altered pharmacology and sensitivity to intracellular Mg·ATP compared to homomeric TRPM7. Strikingly, the activity of heteromeric TRPM7/M6 channels is independent of intracellular Mg·ATP concentrations, essentially uncoupling channel activity from cellular energy status. Disruption of TRPM6 kinase phosphorylation activity re-introduces Mg·ATP sensitivity to the heteromeric channel similar to that of TRPM7. Thus, TRPM6 modulates the functionality of TRPM7, and the TRPM6 kinase plays a critical role in tuning the phenotype of the TRPM7/M6 channel complex.

TRPM7 and TRPM6 belong to the melastatin-related subfamily of TRP channels and represent unique bifunctional proteins with both ion channel and protein kinase function (1–4). The two proteins are highly homologous to each other with >50% sequence identity. TRPM7- and TRPM6-mediated membrane currents exhibit a

highly nonlinear current-voltage (I/V) relationship with pronounced outward rectification (3, 5). The small inward currents at physiologically relevant negative membrane voltages are carried by divalent cations, including Mg^{2+} and Ca^{2+}, and the large outward currents at positive voltages are due to efflux of monovalent cations (5, 6).

Considerable efforts have been directed towards understanding the physiological functions of TRPM7 (7). TRPM7 represents the only known ion channel that is essential for cell viability (3, 8, 9). Its channel function is inhibited by both intracellular free Mg^{2+} and Mg·ATP (3, 10) and both factors serve as the major physiological mechanisms controlling TRPM7-mediated divalent cation transport. Information is more limited for TRPM6 and some of it remains controversial. Conflicting results have been reported concerning TRPM6 expression in heterologous expression systems. Two independent groups were able to measure homomeric TRPM6 currents in HEK-293 cells (5, 11–13), whereas the other two show that TRPM6 is retained intracellularly when expressed alone (14–17). Hence, it has been proposed that TRPM6 may function in association with TRPM7 by forming a heteromeric TRPM7/M6 channel complex (14–17). Channel kinase heteromerization results in a slightly altered permeation and pharmacology profile, pH sensitivity and single channel conductance (11, 12). However, important questions about regulation and functionality of heteromeric channel kinases remain unresolved.

EXPERIMENTAL PROCEDURES

Cell culture and transfection

Wild-type HEK-293 cells were grown in DMEM medium supplemented with 10% fetal bovine serum (FBS) (Invitrogen, USA). The cells were transiently transfected with N-terminally hemagglutinin (HA)-tagged human TRPM6 constructs using Lipofectamine 2000 (Invitrogen, USA). Human TRPM6 phosphotransferase-deficient mutant (TRPM6-K1804R) and human TRPM6 Δkinase were made from the original wild-type pCINeo-IRES-GFP-TRPM6 construct (TRPM6-WT, GenBank accession number 017662) and kindly provided by Dr. J. Hoenderop and Dr. R. Bindels (5, 13). Whole-cell patch clamp experiments were carried out 30 hours post-transfection. Expression of various human TRPM6 constructs was identified by green fluorescence.

For expression in tetracycline (tet)-inducible HEK293 cells, human TRPM6 WT and TRPM6 mutants were cloned into the pcDNA5/TO-FLAG vector and human TRPM7 WT into the pcDNA4/TO-HA vector as previously described (8, 17). Tet-inducible HEK-293 cells encoding human TRPM7 + human TRPM6 WT (TRPM7/M6), human TRPM7 + human TRPM6 K1804R (TRPM7/M6 K1804R) and human TRPM7 + human TRPM6 Δkinase (TRPM7/M6 Δkinase) were maintained in DMEM media containing 10% FBS, blasticidin (5 µg/ml), zeocin (0.4 mg/ml) and hygromycin (0.5 mg/ml) (17). Tetracycline-inducible human TRPM7 HEK-293 cells were cultured in DMEM media containing 10% FBS, blasticidin (5 µg/ml) and zeocin (0.4 mg/ml) (8). Tetracycline-inducible human TRPM6 HEK-293 cells were maintained in DMEM media containing 10% FBS, blasticidin (5 µg/ml) and hygromycin (0.5 mg/ml) (Invitrogen, USA) (17). The proteins were induced by adding 1 µg/ml tetracycline to the culture media. Current measurements were performed 14 - 24 hours following tetracycline induction.

RT-PCR

Total RNA was isolated from four replicates of HEK-293 wild-type cells using RNeasy mini kit (Qiagen, USA). SuperScript III First-Strand Synthesis System for RT-PCR (Invitrogen, USA) was used following the manufacturer's procedure to synthesize cDNA from 1 µg of total RNA primed with oligo (dT) primers. Gene-specific primers for TRPM6 (forward primer 5'-TGCCCTGGAACAAGCAATGTCAG-3'; reverse primer 5'- CTTTTCATCAGCACAGCCCAAACC -3'), TRPM7 (forward primer 5'-AGCATACAGAACAGAGCCCAACGG -3'; reverse primer 5'-TTCCAACAGTGCCATCATCCACC-3'), and GAPDH (forward primer 5'-GGAGCCAAAAGGGTCATCATCTC-3'; reverse primer 5'- AGTGGGTGTCGCTGTTGAAGTC-3')

were designed using MacVector and synthesized by Invitrogen. PCR was performed in reaction volumes of 50 µl containing 1 µl dNTPs (10 mM), 2 µl of each primer (10 pmol/µl), 2 µl cDNA solution, 5 µl of reaction buffer (10x), 37 µl water, and 1 µl Pfu Ultra II fusion HS DNA polymerase (Stratagene) on a Thermal Cycler (BioRad). Denaturation was carried out at 94 °C for 20 seconds, annealing at 55 °C for 30 seconds and elongation at 72 °C for 30 seconds for 35 cycles, followed by extension at 72 °C for 3 minutes. PCR products were detected in 0.8% agarose gel containing 1x SYBR Safe DNA Gel Stain (Invitrogen).

Solutions

To measure TRPM6 currents, cells were kept in an extracellular solution containing (in mM): 140 NaCl, 2.8 KCl, 1 $CaCl_2$, 10 Hepes-NaOH, 11 Glucose; pH 7.4; Current measurements of TRPM7/M6, TRPM7/M6 K1804R and TRPM7/M6 Δkinase were conducted in an extracellular solution composed of (in mM): 140 NaCl, 2.8 KCl, 1 $CaCl_2$, 2 $MgCl_2$, 10 Hepes-NaOH, 11 Glucose; pH 7.4 adjusted with NaOH or HCl.

To test the effects of osmotic challenges on the channels, hypertonic solution was made by adding appropriate quantities of mannitol to the standard external solution while hypotonicity was achieved by reducing the concentration of NaCl from 140 mM to ~90 mM. The control solution for hypotonic solution was made by adjusting the osmolarity to 310 mOsm with appropriate concentration of mannitol. The osmolarities of the solutions were verified by an osmometer (Wescor). Standard internal solution contained (in mM): 140 Cs-glutamate, 8 NaCl, 10 Hepes-CsOH, 10 EGTA-CsOH; pH 7.2 adjusted with CsOH or HCl. In some cases, the strong Mg^{2+} chelator (EDTA) was employed either to entirely remove internal Mg^{2+} or to attain more accuracy in calculating internal free Mg^{2+} concentrations. The free Mg^{2+} levels in pipette solutions were calculated with WebMaxC Standard (http://www.stanford.edu/~cpatton/webmaxcS.htm). The detailed compositions of the pipette solutions for current recordings are shown in tables 1-5. All chemicals were from Sigma Aldrich, USA.

Electrophysiology

Patch-clamp experiments were performed under a tight-seal whole-cell configuration at room temperature (20-25 °C). High-resolution whole-cell currents were recorded by EPC9 (HEKA, Lambrecht, Germany) and Patchmaster v2.4 (HEKA, Lambrecht, Germany). Unless otherwise stated, all voltages were corrected for a liquid junction potential of 10 mV. Patch pipettes pulled from borosilicate glass had resistances of 1.5-2.5 MΩ when filled with internal solutions. Voltage ramps of 50 ms duration spanning a voltage range of -100 mV to +100 mV were applied to the cells from a holding potential of 0 mV at a rate of 0.5 Hz following the establishment of whole-cell configuration. The currents were filtered at 2.9 kHz and digitized at 10 kHz. Currents were analyzed with FitMaster v2.11 (HEKA, Lambrecht, Germany) and Igor Pro (Wavemetrics, Portland, USA). Inward currents were extracted at -80 mV and outward currents at +80 mV. Data were normalized to cell size as current density (pA/pF). All data are given as mean ± standard error of mean (s.e.m.).

RESULTS

Differential pharmacological modulation of homomeric and heteromeric channel kinases

Homomeric TRPM6 and TRPM7 have essentially identical I/V characteristics (3, 5), which makes it challenging to functionally differentiate between these two proteins. Interestingly, 2-aminoethoxydiphenyl borate (2-APB) inhibits TRPM7 and facilitates TRPM6 (11). This prompted us to assess 2-APB on heteromeric TRPM7/M6 currents using tetracycline-sensitive HEK-293 cell lines inducibly overexpressing either human TRPM7 (TRPM7) (8, 17), human TRPM6 (TRPM6) or both TRPM7 and TRPM6 co-expressed (TRPM7/M6) (17). The whole-cell patch clamp technique was used with solutions designed to maximally activate the channels by supplementing intracellular solutions with 10 mM EDTA and using Mg^{2+}-free external solutions.

Within 30 s after whole-cell break-in, both TRPM7 (Fig. 1E) and TRPM7/M6 (Fig. 1C-D) expressing HEK-293 cells (HEK-TRPM7; HEK-

TRPM7/M6) developed large currents with the characteristic outwardly rectifying I/V relationship typical for heterologously overexpressed channels. However, cells overexpressing TRPM6 alone had almost identical current sizes and kinetics of current development compared to uninduced cells (Fig. 1F), consistent with previous biochemical analyses on these cells showing that the majority of overexpressed TRPM6 localizes intracellularly (17). These results are also consistent with observation made in previous attempts to overexpress TRPM6, including various alternative vectors (14, 16, 17). Transient transfection of both TRPM6 and TRPM7 using the pcDNA3.1 vector in HEK-293 cells produced plasma membrane insertion of TRPM6 only in the presence of TRPM7, but not with any other TRPM channel (M1, M2, M4, M5) (14). Similarly, cloning of TRPM6 and TRPM7 into the pcDNA5/TO-Flag plasmid confirmed the inability to overexpress TRPM6 alone in the chicken DT40 and HEK-293 cell systems (17). Moreover, an alternate method using cRNA of TRPM6 injected in *X. laevis* showed that TRPM6 and TRPM7 only overexpress in tandem (14).

We therefore resorted to transient overexpression of TRPM6 in wild-type HEK-293 cells using pCINeo-IRES-GFP-TRPM6 (5), which currently is the only expression vector that results in surface expression of monomeric TRPM6 channels, even if this may not be representative of physiological circumstances in native cells. In agreement with previous reports using this vector (5, 11), cells analyzed 30 h post-transfection developed outwardly rectifying currents that had the typical I/V characteristics of TRPM6 (Fig. 1A-B) and were at least 12 times larger than endogenously measured TRPM7-like currents (Fig. 1F) (3). Although it remains unclear as to why this particular vector allows the formation of overexpressed TRPM6 channels in the plasma membrane, it enabled us to assess the effect of 2-APB on TRPM6, TRPM7 and TRPM7/M6 using these four heterologous cell systems (transient TRPM6, inducible TRPM7, TRPM6 and TRPM7/M6). External application of 200 μM 2-APB significantly enhanced TRPM6 currents (Fig. 1A-B) (11). Conversely, TRPM7 currents were markedly blocked by 200 μM 2-APB (Fig. 1E). When TRPM6 and TRPM7 were co-overexpressed upon tetracycline induction, 200 μM 2-APB was without significant effect on TRPM7/M6 currents (Fig. 1C-D). Tetracycline-induction of HEK-TRPM6 cells did not lead to currents above control levels; however, application of 200 μM 2-APB revealed that TRPM6 indeed can be inserted into the plasma membrane, as currents were facilitated rather than inhibited by this compound (Fig. 1F-G). These data indicate that the composition of the heteromeric channel kinase protein determines its overall sensitivity to 2-APB, resulting in an intermediate response phenotype that averages the facilitatory and inhibitory effects of 2-APB on the monomeric channels.

2-APB is an unspecific pharmacological tool interfering with the activity of a variety of ion channels (11, 18–20). In contrast, waixenicin A is a highly potent and specific inhibitor of TRPM7 that does not affect heterologously expressed TRPM6 (21). We tested the compound's efficacy to inhibit overexpressed TRPM7/M6 currents. Perfusing cells with the standard internal solution containing 780 μM free Mg^{2+} revealed that fully activated TRPM7/M6 currents inactivated by about 30% within 400 s (Fig. 2A). Application of 10 μM waixenicin A decreased TRPM7/M6 currents by 72% during that time, and this effect was also evident in the inward currents assessed at -80 mV (Fig. 2A). Repeating the experiment in the absence of intracellular Mg^{2+} did not affect inhibition of heteromeric channels by waixenicin A (Fig. 2B), leading to an overall 40% compound-induced inhibition. This is in strong contrast to currents carried by homomeric TRPM7, where intracellular Mg^{2+} significantly alters the inhibitory efficacy of waixenicin A (21). In addition, TRPM7 currents are completely suppressed within this application time and concentration of waixenicin A. Thus, while TRPM7/M6 heteromeric channels are sensitive to waixenicin A inhibition, they are less so than TRPM7 alone and the compound's inhibitory effect is uncoupled from intracellular Mg^{2+} dependency. The differential behavior of waixenicin A on TRPM7, TRPM6 and

TRPM7/M6 currents may provide an additional pharmacological tool when characterizing TRPM7-like currents in native cells.

Sensitivity of TRPM6 and TRPM7/M6 channels to hypo- and hyper-osmolarity

TRPM7 is sensitive to osmotic challenges in human kidney cells (22). Since TRPM6 is predominantly expressed in the gut and kidney where osmotic changes are common, we tested whether TRPM6 would also be osmo-sensitive. Considering that intracellular Mg^{2+} availability has significant impacts on channel functionality, we delivered the osmotic changes in the absence and presence of intracellular Mg^{2+}. In the presence of 10 mM EDTA, TRPM6 currents were not affected by hypotonic solutions (210 mOsm, Fig. 2C) while hypertonic solutions slightly reduced the currents by 30% (510 mOsm, Fig. 2C). However, an increase in series resistance as a result of cell shrinkage was observed when the cells were exposed to hypertonic solution, which may account for this small decrease in TRPM6 currents. In the presence of 20 μM Mg^{2+} (Fig. 2D), neither hypotonicity (210 mOsm) nor hypertonicity (510 mOsm) had an effect on TRPM6 compared with corresponding controls (isotonic). Collectively, TRPM6 is largely insensitive to osmotic gradients, which is in marked contrast to TRPM7.

We next examined the responses of TRPM7/M6 heteromer to osmotic challenges. In the absence of intracellular Mg^{2+}, TRPM7/M6 behaved similarly to TRPM6 in response to osmotic changes in that 210 mOsm had no effect on currents, and 510 mOsm induced a small reduction of currents by about 30% (Fig. 2E). However, under conditions where internal free Mg^{2+} was adjusted to more physiological levels of 790 μM, TRPM7/M6 regained sensitivity to osmotic gradients in a dose-dependent manner (Fig. 2F). The fitted dose-response curve yielded an IC_{50} of 460 mOsm for osmolarity-mediated suppression of TRPM7/M6 (Fig. 2G; Hill = 3.3), similar to the IC_{50} of 430 mOsm for TRPM7 (22). However, TRPM7/M6 currents were sensitive to osmolarity over a wider range of osmotic gradients compared to TRPM7, as indicated by their distinctly different Hill coefficients (3.3 versus 11, respectively; Fig. 2G). This suggests that Mg^{2+} is required for the osmo-sensitivity of TRPM7/M6 and that heteromeric complex formation results in a more graded response to osmotic change without changing the midpoint of osmotic sensitivity. As will be shown below, this is consistent with the preserved sensitivity of heteromeric channels to intracellular Mg^{2+}, as a significant factor in mediating osmosensitivity is caused by molecular crowding of inhibitory molecules due to changes in cell volume (22).

Inhibition of homomeric and heteromeric channel kinases by intracellular Mg^{2+}

Intracellular Mg^{2+} regulates both TRPM6 and TRPM7 (3, 5, 8, 10). The IC_{50} for Mg^{2+}-dependent TRPM7 inhibition in the HEK-293 overexpression system is 720 μM in the absence of Mg·ATP (10). However, a complete Mg^{2+} dose-response curve has not yet been determined for native TRPM7 currents in wild-type HEK-293. RT-PCR established that wild-type HEK-293 cells express TRPM7 but did not detect significant TRPM6 (Fig. 3C), suggesting that endogenous conductances are mediated exclusively by TRPM7. As shown in Fig. 3A, B, native TRPM7-like currents were inhibited by intracellular free Mg^{2+} with an IC_{50} of 569 μM, resembling that of heterologously expressed TRPM7 (Fig. 3F) (10). As for TRPM6, Voets *et al* reported an IC_{50} of 510 μM for Mg^{2+} block as determined by means of flash photolysis of caged Mg^{2+} (5). We re-assessed the Mg^{2+} sensitivity of TRPM6 using our standard whole-cell patch clamp approach to allow comparison between data sets obtained from TRPM7, TRPM6 and TRPM7/M6. We used 10 mM EDTA as the internal Mg^{2+} chelator and $MgCl_2$ was calculated to achieve the desired free Mg^{2+} concentrations. Without internal Mg^{2+}, transiently overexpressed TRPM6 currents assessed in HEK-293 cells rapidly activated within 30 s after break-in (Fig. 1A, 3D). Just 10 μM Mg^{2+} significantly suppressed the current size of TRPM6 and 300 μM Mg^{2+} almost abolished the currents (Fig. 3D). The fitted dose-response curve yielded an IC_{50} of 29 μM with a Hill coefficient of 0.7 (Fig. 3F), which is almost 25-fold more sensitive compared to TRPM7 (IC_{50} = 720 μM) (10). We next investigated the Mg^{2+} block of TRPM7/M6 heteromers in the tetracycline-inducible system (17) and determined the Mg^{2+} dose-response curve with intracellular free Mg^{2+} buffered with EGTA to various concentrations. As

shown in the Fig. 3E, intracellular Mg^{2+} dose-dependently blocked TRPM7/M6 currents. The IC_{50} fitted from the dose-response curve for TRPM7/M6 approximated 466 μM with a Hill coefficient of 0.8 (Fig. 3F). The differences in IC_{50} values between native and overexpressed TRPM7 as well as TRPM7/M6 did not amount to statistical significance, although there might be a trend to slightly higher sensitivity of heteromeric channels to Mg^{2+} compared to monomeric TRPM7. However, TRPM7/M6 complexes are dramatically less sensitive to Mg^{2+} (~16-fold decrease) than TRPM6 homomers.

Previous work has demonstrated that the Mg^{2+} sensitivity of monomeric TRPM7 channels is affected by the kinase domain, as kinase-dead point mutations reduce and kinase deletion mutants increase Mg^{2+} sensitivity (8). Two approaches were utilized to eliminate the function of TRPM6 kinase: mutation of a critical amino acid for the phosphotransferase activity (K1804R, TRPM6-K1804R) and removal of the entire kinase domain (TRPM6-Δkinase) in the overexpressed proteins (17). We first determined the Mg^{2+} sensitivity of both homomeric TRPM6-K1804R and TRPM6-Δkinase channels. Both of these TRPM6 mutants were strongly suppressed by Mg^{2+} similar to TRPM6-WT (Fig. 4A, B). Current normalization revealed that TRPM6-K1804R is slightly less sensitive to Mg^{2+} while TRPM6-Δkinase is more sensitive compared with TRPM6-WT (Fig. 4C). This clarifies that TRPM6-WT and its kinase mutants all remain highly sensitive to Mg^{2+} block.

Next we analyzed heteromeric combinations of these subunits with TRPM7 and constructed dose-response curves for TRPM7/M6-KR and TRPM7/M6-Δkinase. As shown in Fig. 4D, E, TRPM7/M6-KR currents and TRPM7/M6-Δkinase currents were dose-dependently suppressed by intracellular Mg^{2+}, but with significantly lower sensitivity compared to homomeric assemblies of TRPM6 with an apparent IC_{50} of 654 μM and 638 μM, respectively (Fig. 4F). Thus, loss of function of the TRPM6 kinase rendered TRPM7/M6-KR slightly less sensitive to Mg^{2+} block than TRPM7/M6-WT (IC_{50} = 466 μM), with a phenotype reminiscent of TRPM7 (10). Even though the slight rightward shifts in sensitivity of the kinase-deficient mutants were not statistically significant, they appear to reverse the slight leftward trend observed in the TRPM7/M6-WT combination, despite their strong Mg^{2+} sensitivity when expressed as homomers.

The TRPM6 kinase domain confers insensitivity of TRPM7/M6 heteromeric channels to intracellular Mg·ATP

Mg·ATP is an important regulator involved in setting TRPM7 activity that synergizes with free Mg^{2+} to suppress TRPM7 (10). With intracellular free Mg^{2+} at 780 μM, the IC_{50} for Mg·ATP inhibition of TRPM7 currents is around 2 mM. In contrast, modulation of TRPM6 by intracellular ATP reportedly occurs independent of Mg^{2+} with an IC_{50} of 1.3 mM and requires an intact kinase domain (13). Both TRPM7 and TRPM6 kinases need the presence of some Mg^{2+} to maintain phosphotransferase activity (3, 8, 23, 24). We therefore adopted an experimental strategy aimed at preserving the kinase activity by including low levels of free Mg^{2+} in the pipette solution. Based on the obtained IC_{50} for Mg^{2+}-mediated TRPM6 suppression, internal free Mg^{2+} was set to 25 μM and 20 μM for testing Mg·ATP and Na·ATP, respectively. Surprisingly, and in contrast to a previous study (13), we found that under these conditions Mg·ATP (3 mM or 9 mM) was completely ineffective to suppress transiently expressed TRPM6 currents (Fig. 5A). Not only that, but the currents remained stable after reaching a plateau, suggesting that ATP prevents current run down and thus may play a role in potentiating channel function. Similar to Mg·ATP, inclusion of Na·ATP (3 mM & 9 mM) in the patch pipette did not block TRPM6 currents but rather resulted in removal of current inactivation (Fig. 5B). Since activation and inactivation processes may compete with each other depending on the presence of ATP and Mg^{2+}, a greater spread of maximal current amplitudes across individually patched cells can be observed in Fig. 5A and 5B. We conclude that Na·ATP and Mg·ATP have similar effects on TRPM6: they do not inhibit TRPM6 homomeric channels and remove TRPM6 inactivation. We have no simple explanation for the conflicting observations made here compared

with those of a previous study that found a Mg^{2+}-independent inhibition of TRPM6 with an IC_{50} of 1.3 mM (13), which would indicate an even higher ATP-sensitivity than that of TRPM7. As will be shown below, we not only see the absence of ATP-dependent inhibition in homomeric TRPM6, but this property of TRPM6 is also conferred on heteromeric TRPM7/M6 channels.

We next asked how ATP might remove the inactivation of TRPM6 and considered the possible mechanisms of Mg·ATP on TRPM6 currents, as Mg·ATP is the physiological form of ATP in the cell. ATP-mediated removal of TRPM6 inactivation could potentially be caused by ATP hydrolysis through the kinase domain, be secondary to the generation of ATP metabolites ADP or AMP, or be due to the physical occupation of ATP-binding sites. Two non-hydrolysable structural analogs of ATP, ATPγs (0.3 mM) and AMP-PNP (3 mM), failed to prevent TRPM6 inactivation (Fig. 5E), indicating that ATP binding alone is not responsible for ATP-mediated sustained opening of TRPM6. The intracellular administration of the ATP metabolites AMP (3 mM) or ADP (3 mM) were similarly ineffective (Fig. 5E). Taken together, this suggests that ATP removes TRPM6 inactivation by a mechanism that is dependent upon ATP hydrolysis.

To investigate whether the kinase domain is involved in ATP-mediated regulation of TRPM6, we tested the effects of Mg·ATP on kinase activity-deficient TRPM6 mutants transiently expressed in wild-type HEK-293 cells. After whole-cell break-in TRPM6-K1804R currents developed in a similar manner as TRPM6-WT currents followed by almost complete inactivation over the time course of the experiment (Fig. 5C). Unlike its effects in TRPM6-WT, internal Mg·ATP of 3 mM and 9 mM did not stabilize TRPM6 activity (Fig. 5C). Similar results were obtained when investigating the behavior of TRPM6-Δkinase currents, although the overall current density was smaller in this mutant (Fig. 5D). Thus it appears that a functional kinase domain with intact phosphotransferase activity is responsible for ATP hydrolysis and maintenance of TRPM6 function.

Mg·ATP regulation of heteromeric TRPM7/M6 was examined by using pipette solutions with higher Mg^{2+} levels (753 μM) around the IC_{50} for free Mg^{2+}. Surprisingly, even in the presence of intracellular Mg^{2+}, TRPM7/M6 currents were not affected by perfusion of cells with physiological (4 mM) and even supra-physiological (8 mM) intracellular Mg·ATP (Fig. 5F). This indicates that the formation of heteromeric TRPM7/M6 uncouples channel kinases from cellular energy metabolism. Since the kinase domain of TRPM6 is able to cross-phosphorylate TRPM7 but not vice versa (17), we hypothesized that regulation of TRPM7 by the TRPM6 kinase might be responsible for the functional characteristics of TRPM7/M6, and that the TRPM6 kinase domain could be involved in setting the Mg·ATP sensitivity of the heteromeric channel complex. We tested this in kinase-deficient TRPM6 mutant constructs TRPM6-Δkinase and TRPM6-K1804R (17). Fig. 5H demonstrates that in contrast to TRPM7/M6-WT, TRPM7/M6-K1804R currents were now inhibited by Mg·ATP in a dose-dependent fashion. Furthermore, removal of the TRPM6 kinase domain (TRPM6-Δkinase) made heteromeric channel currents even more sensitive to intracellular Mg·ATP (Fig. 5H). This indicates that TRPM6 kinase-mediated cross-phosphorylation of TRPM7 is mandatory to render TRPM7/M6 heteromers insensitive to cellular ATP fluctuations.

DISCUSSION

We have found that homomeric TRPM6 channels and heteromeric TRPM7/M6 channels exhibit a number of functional and pharmacological differences and are regulated very differently by free Mg^{2+} and Mg·ATP in comparison to homomeric TRPM7 (see Table 6). Particularly, the regulation by Mg·ATP requires a functional TRPM6 kinase domain.

Robust TRPM6 currents could reliably be measured in HEK293 cells transiently transfected with human TRPM6 in pCINeo-IRES-GFP vector. These findings are in line with other reports that used the same TRPM6 construct (13, 25–27). In contrast to the transient expression system, we failed to detect markedly elevated TRPM6 channel activity in the tetracycline-inducible stable TRPM6 HEK293. Here, a previous study demonstrated that without sufficient TRPM7 subunits available, TRPM6 is largely retained

intracellularly (28). Similarly, TRPM6 overexpression using the expression vectors pcDNA3.1 or pINC(SP1)/Hygro did not result in TRPM6 plasma membrane translocation, and neither did cRNA injection into *Xenopus* oocytes based on the pOGII vector (29, 30). We currently cannot explain as to why the only system that seems to drive translocation of TRPM6 to the plasma membrane without the help of TRPM7 is through the pCINeo-IRES-GFP vector. It would be interesting to see whether the non-coding sequence of the TRPM6-pCINeo-IRES-GFP expression construct influences assembly and trafficking of the TRPM6 channel subunits.

Despite these conflicting findings, the highly efficient membrane expression of TRPM6 using the pCINeo-IRES-GFP vector for transient TRPM6 expression provided an opportunity to examine the modulation of homomeric TRPM6 by various physiological regulators, such as intracellular Mg^{2+} and Mg·ATP. We examined the Mg^{2+} sensitivity of homomeric TRPM6 by perfusing cells with defined buffered intracellular Mg^{2+} solutions and obtained an IC_{50} of ~30 μM. This is at variance with the IC_{50} of 510 μM reported previously (5). However, the latter IC_{50} for Mg^{2+} might be due to the different experimental approach using flash photolysis of Mg^{2+}. Since we here found large differences in Mg^{2+}-sensitivity between TRPM7 and TRPM6 under identical experimental conditions, we are confident that the higher Mg^{2+} sensitivity of TRPM6 is a genuine feature of the channel. Physiological levels of intracellular Mg^{2+} are thought to range between 0.5 and 1 mM. This would suggest that homomeric TRPM6 channels, even if expressed natively in epithelial cells, might play a rather limited role as a physiologically functional ion channel.

In contrast to the strong Mg^{2+} sensitivity of TRPM6, Mg·ATP did not suppress TRPM6 currents at all and rather prevented channel inactivation. This is in contrast to previous work reporting that both Na·ATP and Mg·ATP dose-dependently blocked TRPM6 currents in EDTA-buffered, Mg^{2+}-free intracellular pipette solutions (13). This discrepancy might be due to absence of intracellular Mg^{2+} in the latter study, as Mg^{2+} not only acts as an inhibitory modulator of channel kinases, but also a minimal amount of Mg^{2+} seems to be required for proper function of TRPM6 and TRPM7. For example, early evidence uncovered the synergistic regulation of TRPM7 channel activity by Mg and Mg·ATP, where a threshold Mg concentration of at least 200 μM is needed before inhibition of TRPM7 by ATP is gained (31). Furthermore, intracellular Mg^{2+} dictates the inhibitory effectiveness of halides as well as waixenicin A in both TRPM6 and TRPM7 (32, 33), and free Mg^{2+} is required for the phosphotransferase activity of the TRPM7 channel kinase (23). Hence, complete removal of Mg^{2+}, or even Zn^{2+} bound to the kinase domain by a strong chelator such as EDTA might impair channel function and/or regulation.

Our data show that TRPM6 inactivation was completely removed by ATP, implying that ATP provides a positive regulatory mechanism to maintain TRPM6 function. ATP seems to remove TRPM6 inactivation through kinase-dependent ATP hydrolysis, as kinase activity-deficient TRPM6 mutants inactivated independently of the presence or absence of intracellular ATP. Autophosphorylation of TRPM6 by its kinase domain could be one mechanism to prevent current inactivation. Thus, washout of intracellular ATP during whole-cell patch-clamp measurements would result in channel dephosphorylation and lead to channel inactivation, whereas supply of ATP would enable the TRPM6 channel kinase to hydrolyze ATP and maintain the phosphorylation on TRPM6 channels for sustained channel activity. Indeed, massive autophosphorylation has been detected in the serine/threonine-rich region of TRPM6 following ATP stimulation (34). However, further experiments are required to fully understand the mechanisms underlying ATP-mediated effects, for instance, identification of the specific amino acid targets that are autophosphorylated by the kinase domain.

Unlike other TRP channels that form heteromultimers with their close homologs, including TRPC1/4/5 (35), TRPC3/6/7 (35), TRPV5/V6 (36) and TRP1/3 (37), TRPM7 and TRPM6 possess highly homologous Ser/Thr kinase domains at their C termini. It has

previously been shown that the TRPM6 kinase is able to cross-phosphorylate TRPM7 but not *vice versa* (28). Consistent with this observation, we found that disruption of TRPM6 kinase activity attenuated Mg^{2+}-mediated suppression and restored sensitivity to Mg·ATP inhibition in the channel complex of TRPM7 with kinase-defective TRPM6 mutants. Thus, the phenotype of this kinase mutant is reminiscent of homomeric TRPM7, suggesting that TRPM6 shapes the phenotype of TRPM7/M6 via cross-phosphorylation of TRPM7.

To date, the molecular mechanisms governing the assembly of TRPM7 and TRPM6 remain unknown. Based on the structure of TRPM proteins, TRPM7/M6 most likely functions as a heterotetrameric channel complex. Indeed, emerging evidence suggests that both TRPM7 and TRPM6 subunits contribute to the heteromeric channel pore (27, 29, 30), although the exact stoichiometric architecture of TRPM7/M6 remains to be determined (38).

A model where TRPM6 co-assembles with TRPM7 to form a functional Mg^{2+}-influx channels is attractive due to the overlapping expression profile of TRPM7 and TRPM6 (28, 29, 39, 40). TRPM7 is a ubiquitously expressed ion channel, whereas the tissue expression of TRPM6 is much more restricted, predominantly in the intestine and kidney. A growing number of examined cell lines and tissues have been shown to co-express TRPM7 and TRPM6 (29, 41, 42). Our electrophysiological results from the functional point of view support a refined model and provide insights into characteristics and physiological regulation of the TRPM7/M6 channel complex. First, the IC_{50} of 466 μM for Mg^{2+} suppression suggests that TRPM7/M6 may be functional within the range of physiological levels of Mg^{2+}. Second, the complexed channel responds to osmotic challenges with similar sensitivity as TRPM7, but in a more graded fashion, therefore preserving its proposed Mg^{2+} transport efficiency in tissues where large osmotic changes are common. Third, like TRPM6, the heteromeric channel complex is not regulated by cellular ATP, thus leaving channel kinase-mediated divalent-ion influx unaffected by cellular energy metabolism. In comparison with homomeric TRPM7, whose activity is strongly downregulated by physiological levels of intracellular Mg·ATP, heteromeric TRPM7/M6 may be more efficient in regards to transport of Mg^{2+} and other divalent ions. These features indicate that the TRPM7/M6 channel may be more efficient to function as divalent ion influx channels than either TRPM7 or TRPM6 alone. This may in turn affect cellular functions both physiologically and patho-physiologically, e.g., in the case of tumor cell growth.

ACKNOWLEDGEMENTS

The authors would like to thank S. Johne, L. Tsue, M. K. Monteilh-Zoller and C. Maggio for excellent technical support. We would like to thank Dr. David Horgen for provision of waixenicin A. We are also grateful to Dr. Alexey Ryazanov, Dr. René J.M. Bindels for kindly providing pCINeo-IRES-GFP-TRPM6 construct and to Dr. Joost Hoenderop for sharing TRPM6 K1804R and TRPM6 Δkinase mutants. ZZ, HY, JH: execution of experiments, analysis and display. AF, RP, CS and ZZ: conceptualization and design of project. AF, RP, ZZ: preparation and completion of manuscript. The authors declare no conflict of interest. The work was supported by NIH 5R01GM090123 (CS) and NIH P01 GM078195 (AF). Partial support was provided by a private donation by Mrs. Amy Chong (AF).

REFERENCES

1. Walder, R. Y., Landau, D., Meyer, P., Shalev, H., Tsolia, M., Borochowitz, Z., Boettger, M. B., Beck, G. E., Englehardt, R. K., Carmi, R., and Sheffield, V. C. (2002) Mutation of TRPM6 causes familial hypomagnesemia with secondary hypocalcemia. *Nat. Genet.* 31, 171–174
2. Schlingmann, K. P., Weber, S., Peters, M., Niemann Nejsum, L., Vitzthum, H., Klingel, K., Kratz, M., Haddad, E., Ristoff, E., Dinour, D., Syrrou, M., Nielsen, S., Sassen, M., Waldegger, S., Seyberth, H. W., and Konrad, M. (2002) Hypomagnesemia with secondary hypocalcemia is caused

by mutations in TRPM6, a new member of the TRPM gene family. *Nat. Genet.* 31, 166–170
3. Nadler, M. J., Hermosura, M. C., Inabe, K., Perraud, A. L., Zhu, Q., Stokes, A. J., Kurosaki, T., Kinet, J. P., Penner, R., Scharenberg, A. M., and Fleig, A. (2001) LTRPC7 is a Mg·ATP-regulated divalent cation channel required for cell viability. *Nature* 411, 590–595
4. Runnels, L. W., Yue, L., and Clapham, D. E. (2001) TRP-PLIK, a bifunctional protein with kinase and ion channel activities. *Science* 291, 1043–1047
5. Voets, T., Nilius, B., Hoefs, S., van der Kemp, A. W. C. M., Droogmans, G., Bindels, R. J. M., and Hoenderop, J. G. J. (2004) TRPM6 forms the Mg^{2+} influx channel involved in intestinal and renal Mg^{2+} absorption. *J. Biol. Chem.* 279, 19–25
6. Monteilh-Zoller, M. K., Hermosura, M. C., Nadler, M. J. S., Scharenberg, A. M., Penner, R., and Fleig, A. (2003) TRPM7 provides an ion channel mechanism for cellular entry of trace metal ions. *J. Gen. Physiol.* 121, 49–60
7. Paravicini, T. M., Chubanov, V., and Gudermann, T. (2012) TRPM7: a unique channel involved in magnesium homeostasis. *Int. J. Biochem. Cell Biol.* 44, 1381–1384
8. Schmitz, C., Perraud, A.-L., Johnson, C. O., Inabe, K., Smith, M. K., Penner, R., Kurosaki, T., Fleig, A., and Scharenberg, A. M. (2003) Regulation of vertebrate cellular Mg^{2+} homeostasis by TRPM7. *Cell* 114, 191–200
9. Penner, R., and Fleig, A. (2007) The Mg^{2+} and Mg^{2+}-nucleotide-regulated channel-kinase TRPM7. *Handb. Exp. Pharmacol.* 179, 313–328
10. Demeuse, P., Penner, R., and Fleig, A. (2006) TRPM7 channel is regulated by magnesium nucleotides via its kinase domain. *J. Gen. Physiol.* 127, 421–434
11. Li, M., Jiang, J., and Yue, L. (2006) Functional characterization of homo- and heteromeric channel kinases TRPM6 and TRPM7. *J. Gen. Physiol.* 127, 525–537
12. Li, M., Du, J., Jiang, J., Ratzan, W., Su, L.-T., Runnels, L. W., and Yue, L. (2007) Molecular determinants of Mg^{2+} and Ca^{2+} permeability and pH sensitivity in TRPM6 and TRPM7. *J. Biol. Chem.* 282, 25817–25830
13. Thebault, S., Cao, G., Venselaar, H., Xi, Q., Bindels, R. J., and Hoenderop, J. G. (2008) Role of the alpha-kinase domain in transient receptor potential melastatin 6 channel and regulation by intracellular ATP. *J. Biol. Chem.* 283, 19999–20007
14. Chubanov, V., Waldegger, S., Mederos y Schnitzler, M., Vitzthum, H., Sassen, M. C., Seyberth, H. W., Konrad, M., and Gudermann, T. (2004) Disruption of TRPM6/TRPM7 complex formation by a mutation in the TRPM6 gene causes hypomagnesemia with secondary hypocalcemia. *Proc. Natl. Acad. Sci. U.S.A.* 101, 2894–2899
15. Chubanov, V., Mederos y Schnitzler, M., Wäring, J., Plank, A., and Gudermann, T. (2005) Emerging roles of TRPM6/TRPM7 channel kinase signal transduction complexes. *Naunyn Schmiedebergs Arch. Pharmacol.* 371, 334–341
16. Chubanov, V., Schlingmann, K. P., Wäring, J., Heinzinger, J., Kaske, S., Waldegger, S., Schnitzler, M. M. y, and Gudermann, T. (2007) Hypomagnesemia with secondary hypocalcemia due to a missense mutation in the putative pore-forming tegion of TRPM6. *J. Biol. Chem.* 282, 7656–7667
17. Schmitz, C., Dorovkov, M. V., Zhao, X., Davenport, B. J., Ryazanov, A. G., and Perraud, A.-L. (2005) The channel kinases TRPM6 and TRPM7 are functionally nonredundant. *J. Biol. Chem.* 280, 37763–37771
18. Peinelt, C., Lis, A., Beck, A., Fleig, A., and Penner, R. (2008) 2-Aminoethoxydiphenyl borate directly facilitates and indirectly inhibits STIM1-dependent gating of CRAC channels. *J. Physiol. (Lond.)* 586, 3061–3073
19. Zhang, S. L., Kozak, J. A., Jiang, W., Yeromin, A. V., Chen, J., Yu, Y., Penna, A., Shen, W., Chi, V., and Cahalan, M. D. (2008) Store-dependent and -independent modes regulating Ca^{2+} release-activated Ca^{2+} channel activity of human Orai1 and Orai3. *J. Biol. Chem.* 283, 17662–17671
20. Hu, H., Grandl, J., Bandell, M., Petrus, M., and Patapoutian, A. (2009) Two amino acid residues

determine 2-APB sensitivity of the ion channels TRPV3 and TRPV4. *Proc. Natl. Acad. Sci. U.S.A.* 106, 1626–1631
21. Zierler, S., Yao, G., Zhang, Z., Kuo, W. C., Pörzgen, P., Penner, R., Horgen, F. D., and Fleig, A. (2011) Waixenicin A inhibits cell proliferation through magnesium-dependent block of transient receptor potential melastatin 7 (TRPM7) channels. *J. Biol. Chem.* 286, 39328–39335
22. Bessac, B. F., and Fleig, A. (2007) TRPM7 channel is sensitive to osmotic gradients in human kidney cells. *J. Physiol. (Lond.)* 582, 1073–1086
23. Ryazanova, L. V., Dorovkov, M. V., Ansari, A., and Ryazanov, A. G. (2004) Characterization of the protein kinase activity of TRPM7/ChaK1, a protein kinase fused to the transient receptor potential ion channel. *J. Biol. Chem.* 279, 3708–3716
24. Runnels, L. W. (2011) TRPM6 and TRPM7: A Mul-TRP-PLIK-cation of channel functions. *Curr. Pharm. Biotechnol.* 12, 42–53
25. Voets, T., Nilius, B., Hoefs, S., van der Kemp, A. W., Droogmans, G., Bindels, R. J., and Hoenderop, J. G. (2004) TRPM6 forms the Mg2+ influx channel involved in intestinal and renal Mg2+ absorption. *J. Biol. Chem.* 279, 19–25
26. Li, M., Jiang, J., and Yue, L. (2006) Functional characterization of homo- and heteromeric channel kinases TRPM6 and TRPM7. *J. Gen. Physiol.* 127, 525–37
27. Li, M., Du, J., Jiang, J., Ratzan, W., Su, L. T., Runnels, L. W., and Yue, L. (2007) Molecular determinants of Mg2+ and Ca2+ permeability and pH sensitivity in TRPM6 and TRPM7. *J Biol Chem* 282, 25817–30
28. Schmitz, C., Dorovkov, M. V., Zhao, X., Davenport, B. J., Ryazanov, A. G., and Perraud, A. L. (2005) The channel kinases TRPM6 and TRPM7 are functionally nonredundant. *J. Biol. Chem.* 280, 37763–71
29. Chubanov, V., Waldegger, S., Mederos y Schnitzler, M., Vitzthum, H., Sassen, M. C., Seyberth, H. W., Konrad, M., and Gudermann, T. (2004) Disruption of TRPM6/TRPM7 complex formation by a mutation in the TRPM6 gene causes hypomagnesemia with secondary hypocalcemia. *Proc. Natl. Acad. Sci. U.S.A.* 101, 2894–9
30. Chubanov, V., Schlingmann, K. P., Waring, J., Heinzinger, J., Kaske, S., Waldegger, S., Mederos y Schnitzler, M., and Gudermann, T. (2007) Hypomagnesemia with secondary hypocalcemia due to a missense mutation in the putative pore-forming region of TRPM6. *J. Biol. Chem.* 282, 7656–67
31. Demeuse, P., Penner, R., and Fleig, A. (2006) TRPM7 channel is regulated by magnesium nucleotides via its kinase domain. *J Gen Physiol* 127, 421–34
32. Zierler, S., Yao, G., Zhang, Z., Kuo, W. C., Porzgen, P., Penner, R., Horgen, F. D., and Fleig, A. (2011) Waixenicin A inhibits cell proliferation through magnesium-dependent block of transient receptor potential melastatin 7 (TRPM7) channels. *J. Biol. Chem.* 286, 39328–35
33. Yu, H., Zhang, Z., Lis, A., Penner, R., and Fleig, A. (2013) TRPM7 is regulated by halides through its kinase domain. *Cell. Mol. Life Sci.* 70, 2757–2771
34. Clark, K., Middelbeek, J., Morrice, N. A., Figdor, C. G., Lasonder, E., and van Leeuwen, F. N. (2008) Massive autophosphorylation of the Ser/Thr-rich domain controls protein kinase activity of TRPM6 and TRPM7. *PLoS One* 3, e1876
35. Hofmann, T., Schaefer, M., Schultz, G., and Gudermann, T. (2002) Subunit composition of mammalian transient receptor potential channels in living cells. *Proc. Natl. Acad. Sci. U.S.A.* 99, 7461–6
36. Hoenderop, J. G., Voets, T., Hoefs, S., Weidema, F., Prenen, J., Nilius, B., and Bindels, R. J. (2003) Homo- and heterotetrameric architecture of the epithelial Ca2+ channels TRPV5 and TRPV6. *EMBO* 22, 776–85
37. Lintschinger, B., Balzer-Geldsetzer, M., Baskaran, T., Graier, W. F., Romanin, C., Zhu, M. X., and Groschner, K. (2000) Coassembly of Trp1 and Trp3 proteins generates diacylglycerol- and Ca2+-sensitive cation channels. *J. Biol. Chem.* 275, 27799–805
38. Chubanov, V., Mederos y Schnitzler, M., Waring, J., Plank, A., and Gudermann, T. (2005)

Emerging roles of TRPM6/TRPM7 channel kinase signal transduction complexes. *Naunyn Schmiedebergs Arch. Pharmacol.* 371, 334–41
39. Runnels, L. W. (2011) TRPM6 and TRPM7: A Mul-TRP-PLIK-cation of channel functions. *Curr Pharm Biotechnol* 12, 42–53
40. Schlingmann, K. P., and Gudermann, T. (2005) A critical role of TRPM channel-kinase for human magnesium transport. *J. Physiol. (Lond.)* 566, 301–8
41. Groenestege, W. M., Hoenderop, J. G., van den Heuvel, L., Knoers, N., and Bindels, R. J. (2006) The epithelial Mg2+ channel transient receptor potential melastatin 6 is regulated by dietary Mg2+ content and estrogens. *J. Am. Soc. Nephrol.* 17, 1035–43
42. Kunert-Keil, C., Bisping, F., Kruger, J., and Brinkmeier, H. (2006) Tissue-specific expression of TRP channel genes in the mouse and its variation in three different mouse strains. *BMC Genomics* 7, 159

FIGURE LEGENDS

Figure 1. Differential modulation of TRPM6, TRPM7 and TRPM7/M6 channels by 2-APB. Whole-cell currents in HEK-293 cells were measured in an external solution in which Mg^{2+} was omitted but 1mM Ca^{2+} was present to maintain the typical I-V shape. The internal solution was Mg^{2+}-free in the presence of 10 mM EDTA. 200 μM 2-APB was applied to the cells as indicated by the black bars. Currents were analyzed at + 80 mV and – 80 mV for outward and inward currents, respectively. Representative I-V curves were extracted before application of 2-APB for respective channel type. **(A-B)** whole-cell measurement of outward and inward TRPM6 currents in wild type HEK-293 cells transiently transfected with TRPM6 cDNA (n=7). **(C)** Whole cell measurement of co-overexpressed outward and inward TRPM7/M6 currents in HEK-293 cells induced by tetracycline (n=8). Panel D shows representative I-V curves for control uninduced TRPM7/M6 cells (- tet) and induced TRPM7/M6 cells (+ tet) **(E)** Whole-cell measurement of overexpressed outward and inward TRPM7 currents in HEK-293 cells induced with tetracycline (n=8). **(F-G)** Whole-cell measurement of outward TRPM6 currents in tetracycline-inducible HEK-293 cells in the presence (●, induced, n=8) or absence (○, uninduced, n=8) of tetracycline. Panel G shows the typical I-V curve for induced currents (+ tet) prior to 2-APB application. **(H)** The typical I-V curve for current controls in uninduced TRPM6 cells prior to 2-APB application (- tet) is shown.

Figure 2. Magnesium-independent waxenicin A inhibition and sensitivity to osmotic gradients. HEK-TRPM7/M6 cells were induced by tetracycline (A-B & E-F). TRPM6 currents were measured in HEK-293 cells transiently transfected with TRPM6 (C-D). 10 mM EDTA was used to completely remove internal Mg^{2+} (0 $[Mg^{2+}]_i$, C & D) whereas free Mg^{2+} was clamped by 10 mM EGTA (D & F). **(A)** Whole-cell currents in HEK-293 cells were measured in an external solution in which Mg^{2+} was omitted but 1 mM Ca^{2+} was present to maintain the typical I-V shape. The internal solution was clamped to 780 μM $[Mg^{2+}]_i$. Currents were analyzed at + 80 mV and – 80 mV for outward and inward currents, respectively. Current development assessed in TRPM7/M6 tetracycline-induced cells challenged (○; n=5) or not (●; n=5) with 10 μM waixenicin A as indicated by the black bar. **(B)** Current development assessed in TRPM7/M6 tetracycline-induced cells challenged (○; n=8) or not (●; n=9) with 10 μM waixenicin A in the absence of internal Mg^{2+}. **(C)** TRPM6 currents recorded in the absence of internal Mg^{2+}. The bar indicates application of solutions with low (210 mOsm, n=9) or high osmolarity (510 mOsm, n=9). **(D)** TRPM6 currents recorded in the presence of 20 μM Mg^{2+}. The bar indicates application of isotonic (310 mOsm, n=11), hypotonic (210 mOsm, n=8) or hypertonic solutions (510 mOsm, n=9). **(E)** TRPM7/M6 currents in response to hypotonic (210 mOsm, n=5) or hypertonic challenge (510 mOsm, n=5) in the absence of internal Mg^{2+}. **(F-G)** normalized TRPM7/M6 currents measured in the presence of 790 μM Mg^{2+}**.** All currents were normalized to maximum currents at 100 s after break-in. Bars indicate application of various solutions with different osmolarity. The application was started at 150 s but terminated variably depending upon the tested osmolarity. Note that the solid black line is the control for hypotonic solution in which the osmolarity was normalized to 310 mOsm with mannitol. Data plots in the dose-response curve represent n=7, 12, 9, 10, 6 cells for 200, 310, 380, 510, 800 mOsm, respectively. The ratios of currents (250 s versus the starting point of application at 150 s) were plotted versus the osmotic gradients (E). Dashed line represents the dose-response curve for the osmo-sensitivity of TRPM7 channels (reproduced from (22)).

Figure 3. Suppression of native TRPM7, overexpressed TRPM6 and TRPM7/M6 channels by Mg^{2+}. Native whole-cell TRPM7 currents were assessed in wild-type HEK-293 cells. Whole-cell TRPM6 currents (transiently overexpressed in wild-type HEK-293 cells) were recorded in Mg^{2+}-free external solutions, whereas TRPM7/M6 currents (induced by tetracycline) were measured in normal external solution containing 2 mM Mg^{2+}. The chelator EDTA was used to clamp free Mg^{2+} levels for TRPM6 currents. EGTA was the Mg^{2+} chelator for native TRPM7 currents and induced TRPM7/M6 currents. The

detailed composition of the pipette solutions for current recording is shown in Tables 1 and 2. (**A-B**) Mg^{2+} sensitivity of native TRPM7 currents assessed in wild-type HEK-293 cells by whole-cell patch clamping. Plots represent n=7, 8, 10, 11, 4, 4 cells for 0, 70, 210, 790, 1600, 3200 μM Mg^{2+}, respectively. A dose-response fit rendered an IC_{50} of 569 μM with a Hill coefficient of 1.27 (peak currents extracted at 434 s). **(C)** RT-PCR analysis of the expression of native TRPM6 (546bp) and native TRPM7 (519bp) in HEK-293 wild-type cell line, as well as the housekeeping gene, GAPDH (532bp) (lanes 2 through 3). The gene-specific primers for TRPM6 and TRPM7 amplified the same sized bands from heterologously expressed human TRPM6 and TRPM7 plasmids, respectively (lanes 5 and 6). **(D)** Whole-cell patch clamp analysis of Mg^{2+} block of transiently transfected TRPM6. The number of patched cells is 7, 6, 5, 5, 6, 5, 7 for 0, 10, 30, 100, 300, 900, 1200 μM Mg^{2+}, respectively. **(E)** Whole-cell patch clamp analysis of Mg^{2+} block of TRPM7/M6 currents. Plots represent n=12, 7, 7, 7, 11, 8, 6, 5 cells for 0, 20, 70, 210, 790, 1200, 1600, 3200 μM Mg^{2+}, respectively. **(F)** Dose-response curves of Mg^{2+}-mediated suppression of native TRPM7 (long-dash line taken from panel B and normalized to 1), overexpressed TRPM7 (small-dash line reproduced from (10) and normalized to 1), TRPM6 (extracted at 100 s, closed circles, Hill = 0.69) and TRPM7/M6 currents (extracted at 120 s, open circles, Hill = 0.8).

Figure 4. Mg^{2+} sensitivity of TRPM6 phosphotransferase activity-deficient point mutant (TRPM6-K1804R) and TRPM6-Δkinase alone and in channel complex with TRPM7. The detailed composition of the pipette solutions for current recording is shown in Tables 1 and 2. **(A)** Whole-cell patch clamp assessment of Mg^{2+} block of TRPM6-K1804R currents. **(B)** Whole-cell patch clamp assessment of Mg^{2+} block of TRPM6-Δkinase currents. **(C)** Dose-response curves for Mg^{2+} suppression of whole-cell currents carried by various TRPM6 constructs. Data represent peak currents at the indicated Mg^{2+} concentrations normalized to the maximum currents attained at 0 Mg^{2+}. Peak currents extracted at 100 s, 48 s, 48 s were averaged for dose-response analysis for TRPM6 WT, TRPM6 K1804R, TRPM6 Δkinase, respectively. Note that the plots of TRPM6 WT are derived from Fig. 2D. Plots represent n=7, 6, 5, 5, 6, 5, experiments (TRPM6 WT, 0, 10, 30, 100, 300, 900μM Mg^{2+}, respectively), n=5, 5, 5, 5, 5, 5, experiments (K1804R, 0, 10, 30, 100, 300, 900 μM Mg^{2+}, respectively), and n=5, 8, 6 experiments (Δkinase, 0, 30, 100 μM Mg^{2+}, respectively). Panels D-F are from heteromeric channels where HEK-TRPM7/M6-K1804R cells and HEK-TRPM7/M6-Δkinase cells were induced by tetracycline to co-overexpress TRPM7/M6-K1804R and TRPM7/M6-Δkinase, respectively. The internal and external solutions for current recording (D-E) are the same as those for TRPM7/M6 in Fig. 2E. **(D)** Whole-cell patch clamp analysis of Mg^{2+} inhibition of TRPM7/M6 K1804R currents. Pipette solution contained the indicated concentrations of free Mg^{2+}. Plots represent n=8, 9, 6, 6, 6, 5 cells for 0, 20, 210, 790, 1600, 3200 μM Mg^{2+}, respectively. **(E)** Whole-cell patch clamp assessment of Mg^{2+} suppression of induced TRPM7/M6 Δkinase currents. Plots represent n=5, 5, 5, 7, 6, 5 cells for 0, 20, 210, 790, 1600, 3200 μM Mg^{2+}, respectively. **(F)** Dose-response curves for Mg^{2+} suppression of TRPM7/M6 K1804R (peak currents extracted at 76 s, Hill = 1.34) and TRPM7/M6 Δkinase currents (extracted at 136 s Hill = 1.28).

Figure 5. Mg·ATP does not affect the TRPM7/M6 channel complex and rescues TRPM6 from inactivation. Transiently overexpressed TRPM6 currents were measured in HEK-293 cells and in Mg^{2+}-free external solutions (A-D), while tetracycline-inducible currents of TRPM7 plus various TRPM6 mutants were recorded in normal external solution containing 2 mM Mg^{2+} and 1 mM Ca^{2+} (E-G). The intracellular free Mg^{2+} for TRPM6 current recording was 25.4 μM (A, C, D; see Table 3 for composition of pipette solutions) or 20 μM (B; see Table 4 for composition of pipette solutions), and was 753 μM for heteromeric channels of TRPM7 plus TRPM6 (E-G; see Table 5 for composition of pipette solutions). **(A)** HEK-293 cells transiently overexpressing TRPM6 were dialyzed with pipette solutions containing the indicated concentrations of Mg·ATP. Plots represent n= 14, 11, 10 cells for 0, 3, 9 mM Mg·ATP, respectively. **(B)** Na·ATP rather than Mg·ATP was tested in TRPM6 WT. Plots were averaged from 10, 10, 9 cells for 0, 3, 9 mM Mg·ATP, respectively. **(C)** TRPM6 K1804R mutant was transiently over-

expressed. Plots represent n=7, 7, 9 cells for 0, 3, 9 mM Mg·ATP, respectively. **(D)** The effects of Mg·ATP on TRPM6 Δkinase mutant were tested in HEK-293 cells transiently overexpressing the mutant channel. Internal solutions had the same composition as in A & C. Plots represent n=7, 8, 9 cells for 0, 3, 9 mM Mg·ATP, respectively. **(E)** Normalized to current peak percent inactivation of transiently expressed TRPM6 WT in HEK293. Cells were perfused with either no addition of Mg·ATP (control, n = 14, see panel A), 3 mM (n = 11, panel A) or 9 mM Mg·ATP (n = 10, panel A), 3 mM AMP-PNP (n = 13), 3 mM ADP (n = 9), 3 mM AMP (n = 12) or 300 μM ATPγS (n = 9). **(F)** Whole-cell TRPM7/M6 currents measured at 753 μM Mg^{2+} under the indicated conditions. Plots are representative of 14, 19, 19 cells for 0, 4, 8 mM Mg·ATP, respectively. **(G)** Whole-cell currents of TRPM7/M6 K1804R co-expressed mutant channel complex measured at 753 μM Mg^{2+} under the indicated conditions. Plots represent n=17, 14, 16 cells for 0, 4, 8 mM Mg·ATP, respectively. **(H)** Whole-cell recording of tetracycline induced TRPM7/M6 Δkinase mutant complex currents at 753 μM free Mg^{2+} under the indicated conditions. Note that the experimental conditions in E, F, G are identical. The number of patched cells is 9, 13, 9 for 0, 4, 8 mM Mg·ATP, respectively.

TABLES

Table 1

free $[Mg^{2+}]_i$	Cs-glutamate	NaCl	Cs-Hepes	Cs-EDTA	$MgCl_2$	NMDG-Cl
0	120	8	10	10	0	22.34
0.01	120	8	10	10	7.58	7.18
0.03	120	8	10	10	9.07	4.20
0.1	120	8	10	10	9.79	2.76
0.3	120	8	10	10	10.19	1.96
0.9	120	8	10	10	10.86	0.62
1.2	120	8	10	10	11.17	0

Table 1. Internal solution for Mg^{2+} dose-response curve of TRPM6 WT, TRPM6 K1804R and TRPM6 Δkinase (in mM; pH 7.2). The Cl^- concentration among all solutions is ~30.34 mM.

Table 2

free $[Mg^{2+}]_i$	Cs-glutamate	NaCl	Cs-Hepes	Cs-EGTA	$MgCl_2$
0	140	8	10	10	0
0.02	140	8	10	10	0.0298
0.07	140	8	10	10	0.105
0.21	140	8	10	10	0.313
0.79	140	8	10	10	1.167
1.2	140	8	10	10	1.761
1.6	140	8	10	10	2.334
3.2	140	8	10	10	4.568

Table 2. Internal solution for Mg^{2+} dose-response curve of TRPM7/M6, TRPM7/M6 K1804R and TRPM7/M6 Δkinase (in mM; pH 7.2)

Table 3

Cs-glutamate	NaCl	Cs-Hepes	Cs-EDTA	$MgCl_2$	Mg·ATP
140	8	10	2.00	1.8	0
140	8	10	2.70	0	3
140	8	10	8.15	0	9

Table 3. Internal solution for Mg·ATP effects on TRPM6 WT, TRPM6 K1804R and TRPM6 Δkinase (in mM; pH 7.2). The free Mg^{2+} is ~25.4 µM.

Table 4

Cs-Glutamate	NaCl	Cs-Hepes	Cs-EGTA	$MgCl_2$	Na·ATP
140	8	10	10	0.03	0
140	8	10	10	0.5	3
140	8	10	10	1.45	9

Table 4. Internal solution for Na·ATP effects on TRPM6 WT (in mM; pH 7.2). The free Mg^{2+} is ~20 µM and the total complexed Mg·ATP under these conditions amounts to 0, 0.5, and 1.4 mM, respectively.

Table 5

Cs-glutamate	NaCl	Cs-Hepes	Cs-EGTA	$MgCl_2$	Mg·ATP
140	8	10	10	1.11	0
140	8	10	10	0.55	4.51
140	8	10	10	0	9

Table 5. Internal solution for Mg·ATP effects on TRPM7/M6, TRPM7/M6 K1804R and TRPM7/M6 Δkinase (in mM; pH 7.2). The free Mg^{2+} is ~753 µM and the total complexed Mg·ATP under these conditions amounts to 0, 4, and 8 mM, respectively.

Table 6

Regulation by	**TRPM7**	**TRPM7/M6**	**TRPM6**
free Mg^{2+} (IC_{50})	720 µM (10)	466 µM	29 µM
Mg·ATP (IC_{50})	2-3 mM (10)	no effect	no effect
Osmolarity (IC_{50} / Hill coeff.)	430 mOsm / 11 (22)	460 mOsm / 3.3	no effect
2-APB (200 µM)	block	no effect	facilitation
Waixenicin A (10 µM)	full block (21)	partial block	no effect (21)

Table 6. Summary of salient effects of various regulators of TRPM7, TRPM6, and TRPM7/M6. Data are taken from present manuscript unless indicated by reference.

FIGURES

Figure 1

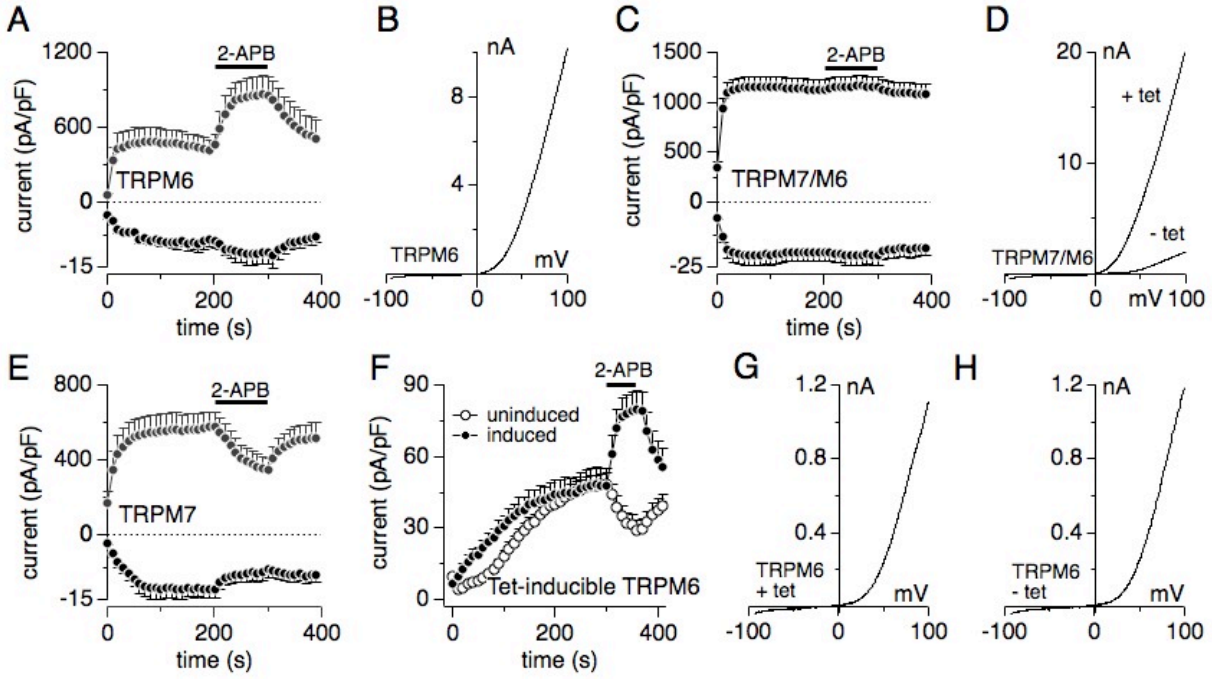

Figure 1. Differential modulation of TRPM6, TRPM7 and TRPM7/M6 channels by 2-APB. Whole-cell currents in HEK-293 cells were measured in an external solution in which Mg^{2+} was omitted but 1mM Ca^{2+} was present to maintain the typical I-V shape. The internal solution was Mg^{2+}-free in the presence of 10 mM EDTA. 200 µM 2-APB was applied to the cells as indicated by the black bars. Currents were analyzed at + 80 mV and – 80 mV for outward and inward currents, respectively. Representative I-V curves were extracted before application of 2-APB for respective channel type. **(A-B)** whole-cell measurement of outward and inward TRPM6 currents in wild type HEK-293 cells transiently transfected with TRPM6 cDNA (n=7). **(C)** Whole cell measurement of co-overexpressed outward and inward TRPM7/M6 currents in HEK-293 cells induced by tetracycline (n=8). Panel D shows representative I-V curves for control uninduced TRPM7/M6 cells (- tet) and induced TRPM7/M6 cells (+ tet) **(E)** Whole-cell measurement of overexpressed outward and inward TRPM7 currents in HEK-293 cells induced with tetracycline (n=8). **(F-G)** Whole-cell measurement of outward TRPM6 currents in tetracycline-inducible HEK-293 cells in the presence (●, induced, n=8) or absence (○, uninduced, n=8) of tetracycline. Panel G shows the typical I-V curve for induced currents (+ tet) prior to 2-APB application. **(H)** The typical I-V curve for current controls in uninduced TRPM6 cells prior to 2-APB application (- tet) is shown.

Figure 2

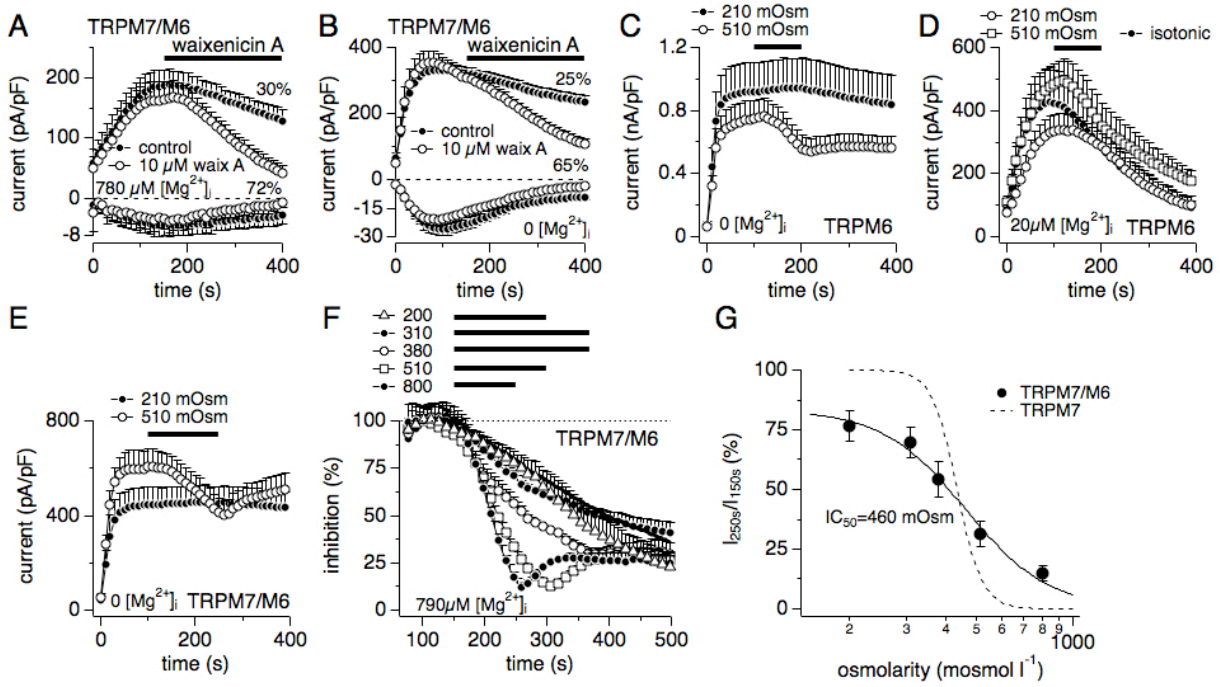

Figure 2. Magnesium-independent waxenicin A inhibition and sensitivity to osmotic gradients. HEK-TRPM7/M6 cells were induced by tetracycline (A-B & E-F). TRPM6 currents were measured in HEK-293 cells transiently transfected with TRPM6 (C-D). 10 mM EDTA was used to completely remove internal Mg^{2+} (0 $[Mg^{2+}]_i$, C & D) whereas free Mg^{2+} was clamped by 10 mM EGTA (D & F). **(A)** Whole-cell currents in HEK-293 cells were measured in an external solution in which Mg^{2+} was omitted but 1 mM Ca^{2+} was present to maintain the typical I-V shape. The internal solution was clamped to 780 µM $[Mg^{2+}]_i$. Currents were analyzed at + 80 mV and – 80 mV for outward and inward currents, respectively. Current development assessed in TRPM7/M6 tetracycline-induced cells challenged (○; n=5) or not (●; n=5) with 10 µM waixenicin A as indicated by the black bar. **(B)** Current development assessed in TRPM7/M6 tetracycline-induced cells challenged (○; n=8) or not (●; n=9) with 10 µM waixenicin A in the absence of internal Mg^{2+}. **(C)** TRPM6 currents recorded in the absence of internal Mg^{2+}. The bar indicates application of solutions with low (210 mOsm, n=9) or high osmolarity (510 mOsm, n=9). **(D)** TRPM6 currents recorded in the presence of 20 µM Mg^{2+}. The bar indicates application of isotonic (310 mOsm, n=11), hypotonic (210 mOsm, n=8) or hypertonic solutions (510 mOsm, n=9). **(E)** TRPM7/M6 currents in response to hypotonic (210 mOsm, n=5) or hypertonic challenge (510 mOsm, n=5) in the absence of internal Mg^{2+}. **(F-G)** normalized TRPM7/M6 currents measured in the presence of 790 µM Mg^{2+}**.** All currents were normalized to maximum currents at 100 s after break-in. Bars indicate application of various solutions with different osmolarity. The application was started at 150 s but terminated variably depending upon the tested osmolarity. Note that the solid black line is the control for hypotonic solution in which the osmolarity was normalized to 310 mOsm with mannitol. Data plots in the dose-response curve represent n=7, 12, 9, 10, 6 cells for 200, 310, 380, 510, 800 mOsm, respectively. The ratios of currents (250 s versus the starting point of application at 150 s) were plotted versus the osmotic gradients (E). Dashed line represents the dose-response curve for the osmo-sensitivity of TRPM7 channels (reproduced from (22)).

Figure 3

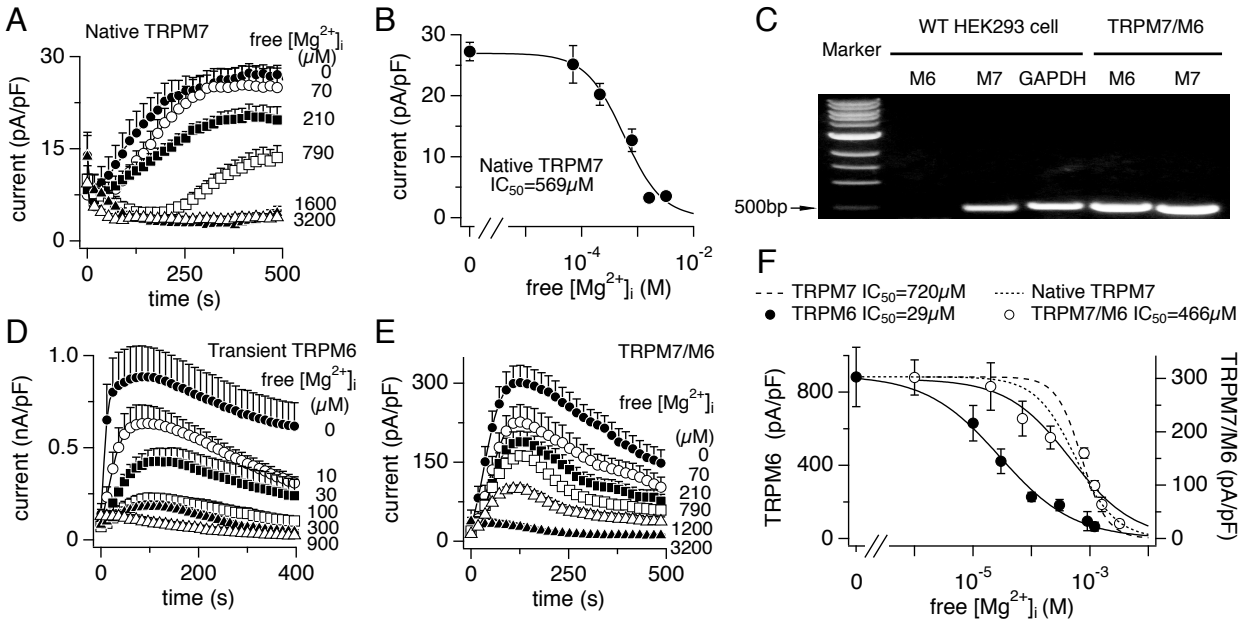

Figure 3. Suppression of native TRPM7, overexpressed TRPM6 and TRPM7/M6 channels by Mg^{2+}. Native whole-cell TRPM7 currents were assessed in wild-type HEK-293 cells. Whole-cell TRPM6 currents (transiently overexpressed in wild-type HEK-293 cells) were recorded in Mg^{2+}-free external solutions, whereas TRPM7/M6 currents (induced by tetracycline) were measured in normal external solution containing 2 mM Mg^{2+}. The chelator EDTA was used to clamp free Mg^{2+} levels for TRPM6 currents. EGTA was the Mg^{2+} chelator for native TRPM7 currents and induced TRPM7/M6 currents. The detailed composition of the pipette solutions for current recording is shown in Tables 1 and 2. (**A-B**) Mg^{2+} sensitivity of native TRPM7 currents assessed in wild-type HEK-293 cells by whole-cell patch clamping. Plots represent n=7, 8, 10, 11, 4, 4 cells for 0, 70, 210, 790, 1600, 3200 μM Mg^{2+}, respectively. A dose-response fit rendered an IC_{50} of 569 μM with a Hill coefficient of 1.27 (peak currents extracted at 434 s). **(C)** RT-PCR analysis of the expression of native TRPM6 (546bp) and native TRPM7 (519bp) in HEK-293 wild-type cell line, as well as the housekeeping gene, GAPDH (532bp) (lanes 2 through 3). The gene-specific primers for TRPM6 and TRPM7 amplified the same sized bands from heterologously expressed human TRPM6 and TRPM7 plasmids, respectively (lanes 5 and 6). **(D)** Whole-cell patch clamp analysis of Mg^{2+} block of transiently transfected TRPM6. The number of patched cells is 7, 6, 5, 5, 6, 5, 7 for 0, 10, 30, 100, 300, 900, 1200 μM Mg^{2+}, respectively. **(E)** Whole-cell patch clamp analysis of Mg^{2+} block of TRPM7/M6 currents. Plots represent n=12, 7, 7, 7, 11, 8, 6, 5 cells for 0, 20, 70, 210, 790, 1200, 1600, 3200 μM Mg^{2+}, respectively. **(F)** Dose-response curves of Mg^{2+}-mediated suppression of native TRPM7 (long-dash line taken from panel B and normalized to 1), overexpressed TRPM7 (small-dash line reproduced from (10) and normalized to 1), TRPM6 (extracted at 100 s, closed circles, Hill = 0.69) and TRPM7/M6 currents (extracted at 120 s, open circles, Hill = 0.8).

Figure 4

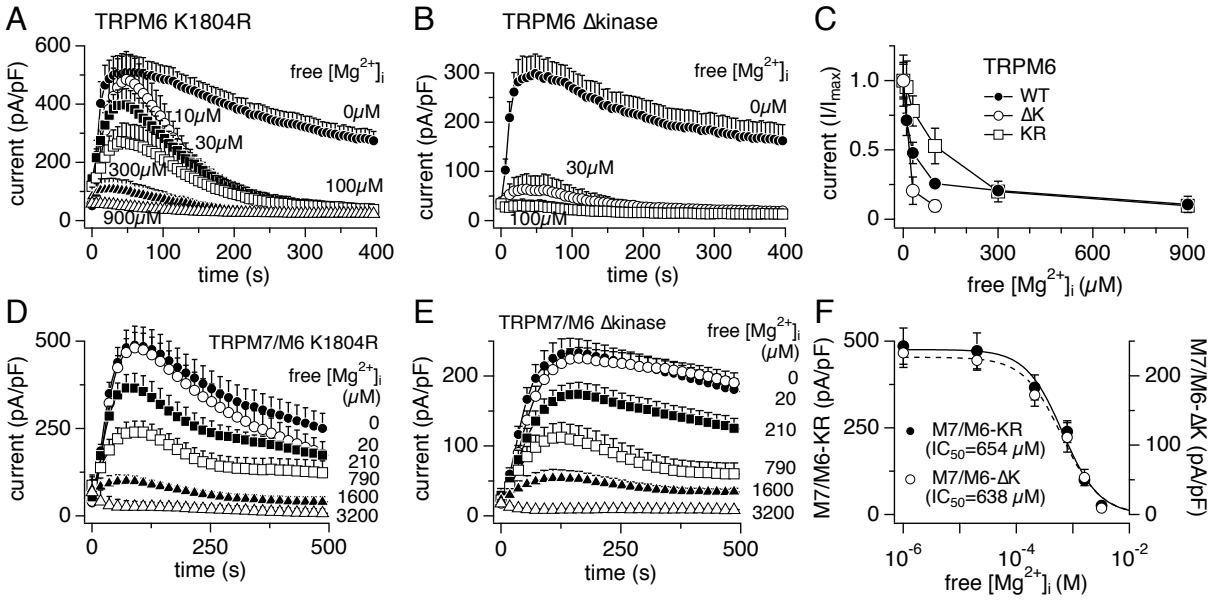

Figure 4. Mg^{2+} sensitivity of TRPM6 phosphotransferase activity-deficient point mutant (TRPM6-K1804R) and TRPM6-Δkinase alone and in channel complex with TRPM7. The detailed composition of the pipette solutions for current recording is shown in Tables 1 and 2. **(A)** Whole-cell patch clamp assessment of Mg^{2+} block of TRPM6-K1804R currents. **(B)** Whole-cell patch clamp assessment of Mg^{2+} block of TRPM6-Δkinase currents. **(C)** Dose-response curves for Mg^{2+} suppression of whole-cell currents carried by various TRPM6 constructs. Data represent peak currents at the indicated Mg^{2+} concentrations normalized to the maximum currents attained at 0 Mg^{2+}. Peak currents extracted at 100 s, 48 s, 48 s were averaged for dose-response analysis for TRPM6 WT, TRPM6 K1804R, TRPM6 Δkinase, respectively. The data for TRPM6 WT are derived from Fig. 2D. Plots represent n=7, 6, 5, 5, 6, 5, experiments (TRPM6 WT, 0, 10, 30, 100, 300, 900μM Mg^{2+}, respectively), n=5, 5, 5, 5, 5, 5, experiments (K1804R, 0, 10, 30, 100, 300, 900 μM Mg^{2+}, respectively), and n=5, 8, 6 experiments (Δkinase, 0, 30, 100 μM Mg^{2+}, respectively). Panels D-F are from heteromeric channels where HEK-TRPM7/M6-K1804R cells and HEK-TRPM7/M6-Δkinase cells were induced by tetracycline to co-overexpress TRPM7/M6-K1804R and TRPM7/M6-Δkinase, respectively. The internal and external solutions for current recording (D-E) are the same as those for TRPM7/M6 in Fig. 2E. **(D)** Whole-cell patch clamp analysis of Mg^{2+} inhibition of TRPM7/M6 K1804R currents. Pipette solution contained the indicated concentrations of free Mg^{2+}. Plots represent n=8, 9, 6, 6, 6, 5 cells for 0, 20, 210, 790, 1600, 3200 μM Mg^{2+}, respectively. **(E)** Whole-cell patch clamp assessment of Mg^{2+} suppression of induced TRPM7/M6 Δkinase currents. Plots represent n=5, 5, 5, 7, 6, 5 cells for 0, 20, 210, 790, 1600, 3200 μM Mg^{2+}, respectively. **(F)** Dose-response curves for Mg^{2+} suppression of TRPM7/M6 K1804R (peak currents extracted at 76 s, Hill = 1.34) and TRPM7/M6 Δkinase currents (extracted at 136 s Hill = 1.28).

Figure 5

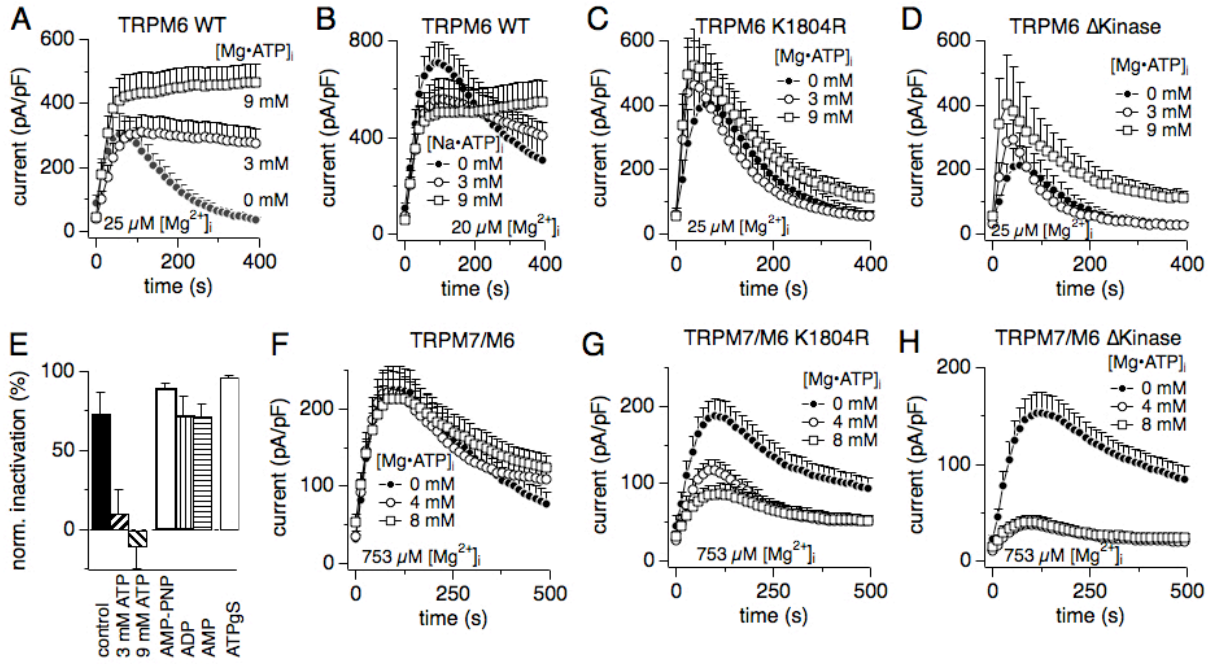

Figure 5. Mg·ATP does not affect the TRPM7/M6 channel complex and rescues TRPM6 from inactivation. Transiently overexpressed TRPM6 currents were measured in HEK-293 cells and in Mg^{2+}-free external solutions (A-D), while tetracycline-inducible currents of TRPM7 plus various TRPM6 mutants were recorded in normal external solution containing 2 mM Mg^{2+} and 1 mM Ca^{2+} (E-G). The intracellular free Mg^{2+} for TRPM6 current recording was 25.4 μM (A, C, D; see Table 3 for composition of pipette solutions) or 20 μM (B; see Table 4 for composition of pipette solutions), and was 753 μM for heteromeric channels of TRPM7 plus TRPM6 (E-G; see Table 5 for composition of pipette solutions). **(A)** HEK-293 cells transiently overexpressing TRPM6 were dialyzed with pipette solutions containing the indicated concentrations of Mg·ATP. Plots represent n= 14, 11, 10 cells for 0, 3, 9 mM Mg·ATP, respectively. **(B)** Na·ATP rather than Mg·ATP was tested in TRPM6 WT. Plots were averaged from 10, 10, 9 cells for 0, 3, 9 mM Mg·ATP, respectively. **(C)** TRPM6 K1804R mutant was transiently over-expressed. Plots represent n=7, 7, 9 cells for 0, 3, 9 mM Mg·ATP, respectively. **(D)** The effects of Mg·ATP on TRPM6 Δkinase mutant were tested in HEK-293 cells transiently overexpressing the mutant channel. Internal solutions had the same composition as in A & C. Plots represent n=7, 8, 9 cells for 0, 3, 9 mM Mg·ATP, respectively. **(E)** Normalized to current peak percent inactivation of transiently expressed TRPM6 WT in HEK293. Cells were perfused with either no addition of Mg·ATP (control, n = 14, see panel A), 3 mM (n = 11, panel A) or 9 mM Mg·ATP (n = 10, panel A), 3 mM AMP-PNP (n = 13), 3 mM ADP (n = 9), 3 mM AMP (n = 12) or 300 μM ATPγS (n = 9). **(F)** Whole-cell TRPM7/M6 currents measured at 753 μM Mg^{2+} under the indicated conditions. Plots are representative of 14, 19, 19 cells for 0, 4, 8 mM Mg·ATP, respectively. **(G)** Whole-cell currents of TRPM7/M6 K1804R co-expressed mutant channel complex measured at 753 μM Mg^{2+} under the indicated conditions. Plots represent n=17, 14, 16 cells for 0, 4, 8 mM Mg·ATP, respectively. **(H)** Whole-cell recording of tetracycline induced TRPM7/M6 Δkinase mutant complex currents at 753 μM free Mg^{2+} under the indicated conditions. Note that the experimental conditions in E, F, G are identical. The number of patched cells is 9, 13, 9 for 0, 4, 8 mM Mg·ATP, respectively.